



## ARTICLE OPEN



# Low temperature chemical sintering of inkjet-printed Zn nanoparticles for highly conductive flexible electronic components

Subimal Majee<sup>1</sup> , Mikael C. F. Karlsson<sup>1,2</sup>, Pawel Jerzy Wojcik<sup>1,3</sup>, Anurak Sawatdee<sup>1</sup>, Mohammad Yusuf Mulla<sup>1</sup>, Naveed ul Hassan Alvi<sup>1</sup>, Peter Dyreklev<sup>1</sup>, Valerio Beni<sup>1</sup> and David Nilsson<sup>1</sup> 

This study illustrates an innovative way to fabricate inkjet-printed tracks by sequential printing of Zn nanoparticle ink and curing ink for low temperature in situ chemical sintering. Employing chemical curing in place of standard sintering methods leads to the advantages of using flexible substrates that may not withstand the high thermal budgets of the standard methods. A general formulation engineering method is adopted to produce highly concentrated Zn ink which is cured by inkjet printing an over-layer of aqueous acetic acid which is the curing agent. The experimental results reveal that a narrow window of acid concentration of curing ink plays a crucial role in determining the electrical properties of the printed Zn nanoparticles. Highly conductive ( $\sim 10^5 \text{ S m}^{-1}$ ) and mechanically flexible printed Zn features are achieved. In addition, from systematic material characterization, we obtain an understanding of the curing mechanism. Finally, a touch sensor circuit is demonstrated involving all-Zn printed conductive tracks.

*npj Flexible Electronics* (2021) 5:14; <https://doi.org/10.1038/s41528-021-00111-1>

## INTRODUCTION

Inkjet-printing of electrodes and connectors using conductive inks has captured much attention in the last couple of decades in various printed electronics applications owing to its non-contact<sup>1,2</sup>, additive, and high-resolution drop-on-demand fabrication ability<sup>3,4</sup>. Not least due to its compatibility with a broad range of substrates and functional inks<sup>1-5</sup>. Nanoparticle (NP) based conductive inks are commonly used in inkjet printing because of the particle size limitation for the inkjet nozzles, scalability of NP production, and dispersibility with high concentrations in the ink carrier fluid<sup>6</sup>. The unprocessed non-dispersed NPs can be sintered at relatively lower temperatures compared to their bulk counterparts due to the high surface area to volume ratio. However, most NP-based inks require additional surfactants and binders to prevent their agglomeration inside the ink carrier fluid. These additives should be removed from the printed films through elevated sintering temperature to achieve required electrical functionalities, hence, sometimes limiting their use to heat-sensitive substrates<sup>2,6</sup>. In most cases, sintering is carried out by transferring the printed samples from the printer stage to curing machinery adding extra processing steps, and causing alignment issues for the subsequent printed layers. Thus, in situ low-temperature sintering of printed NPs on the same printer stage is exciting which leads to advantages of eliminating alignment issues, using flexible substrates that may not withstand the high thermal budgets, reducing the processing steps and overall cost in the device fabrication and opening up opportunities for roll-to-roll inkjet printing possibilities. The important and decisive criteria for the choice of suitable NP conductive inks for specific printed electronics applications are electrical conductivity, oxidation stability, costs, and ink formulation methods. Similarly, sintering conditions and processing steps are also determinative factors<sup>7</sup>. These parameters form the context for the present study.

Although non-metallic inkjet printable conductive inks are available based on conductive polymers such as PEDOT:PSS, and carbonaceous NPs (i.e., graphene); the majority of the conducting inks available in the market rely on metallic NPs (Ag, Au, Cu, Ni)<sup>2,7-13</sup>. The state-of-the-art fabrication of conducting patterns in inkjet-printed electronics is dominated by the use of Ag-based inks. In order to provide electrical functionality to the Ag layer, the printed film must be subjected to highly energetic curing methods such as thermal, NIR, electrical heating, or microwave sintering<sup>2,7</sup>. However, in the case of heat-sensitive substrates (paper, plastic, etc.), most of the earlier stated sintering techniques cannot be applied due to the risk of damage. The Ag ink printed on top of heat-sensitive substrates is curable using laser or photo-sintering<sup>14</sup>. In all the above cases the energy consumption is substantial. Another problem is related to the costs of production. Ag nanoparticle-based inks are widely used because of their high conductivity and good leveling property. However, Ag is too expensive to be employed for low-cost applications. In some cases, the costs of production may be lowered with the application of Cu ink instead of Ag due to the lower material cost. Although roll-to-roll electrodeless deposition of Cu metallic films has been reported by Eastman Kodak which is suitable for deposition on polyethylene terephthalate (PET) substrates<sup>15</sup>. However, the use of Cu deteriorates the performance of the printed tracks because of the presence of the resistive CuO<sub>x</sub>. This significantly increases the contact resistance and shortens the product life due to the progressive oxidation of the Cu film<sup>2,10,16,17</sup>. Inkjet printable Au and Ni NP inks are corrosion resistant with high electrical conductivity. Nevertheless, Au inks are costly compared to the other metallic inks and they need an elevated sintering temperature (200–400 °C) which prevents their use for heat-sensitive substrates. Recently inkjet printable Au NP inks are commercially available that can be cured by photonic sintering process allowing usage on PET substrates, which is,

<sup>1</sup>RISE Research Institutes of Sweden, Norrköping, Sweden. <sup>2</sup>Energy and Environment Science and Technology, Idaho National Laboratory, Idaho Falls, ID, United States. <sup>3</sup>redoxme AB, Research & Development Department, Norrköping, Sweden. <sup>✉</sup>email: subimal.majee@ri.se; david.nilsson@ri.se

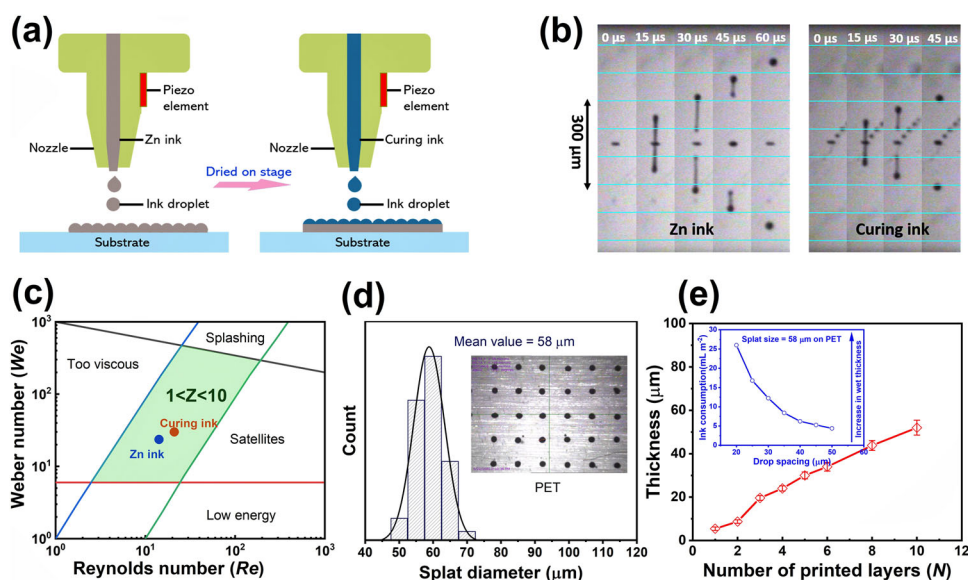


**Fig. 1** Formulation and printing of Zn NP ink and curing ink. **a** Inkjet printing of Zn ink followed by curing ink on PET substrates. **b** Drop formations of the Zn ink and the curing ink from the nozzles, respectively. **c** The dimensionless  $Z$  values of Zn and curing inks in the Weber number vs Reynolds number plot. **d** Splat diameter histogram for Zn ink and the droplets on PET substrate (inset: ink consumption vs drop-spacing estimation). Standard deviations for the thickness measurements are shown as error bars. Lines are guides for the eye.

however, not an energy-efficient process<sup>18</sup>. While commercial Ni inkjet ink is cheaper than Ag and Au inks, Ni NP inks often tend to agglomerate and clog the inkjet printheads<sup>7</sup>. Moreover, curing of Ni NP ink requires either a higher temperature (>350 °C) or a photonic sintering method<sup>12</sup>. Therefore, formulation of inkjet printable alternative conductive metallic NP inks, such as Zn NP ink, is necessary that is inexpensive, curable at low temperature, and highly conductive. The environmental footprint of Zn layers is negligible when comparing with Ag. Zn oxidizes under wet environmental conditions turning into harmless ZnO which is the main component of paints, toothpaste, and many other daily used products. The chemical sintering method of metallic NP inks is an interesting non-conventional route to activate the coalescence of NPs. This method firstly allows us to cure the NPs at low temperature and secondly is an energy-efficient process<sup>19</sup>. Room temperature electrochemical sintering of Zn NP ink by weak acidic treatment has been reported previously by Lee et al.<sup>20</sup>. Utilizing a similar mechanism Jayasayee et al.<sup>21</sup> reported a cost-effective method of preparing porous Zn electrodes for rechargeable zinc–air batteries. In all these cases, a mixture of CH<sub>3</sub>COOH and distilled water (1:10 by volume) was drop-casted either on screen-printed Zn ink or on Zn slurry to enhance the electrical conductivity and other desired functionality. While those reports give a detailed scientific insight into the sintering mechanism, however, the described sintering technique (drop-casting) is unsuitable for large area device manufacturing processes. To the best of our knowledge inkjet printing and low-temperature curing of Zn, NP ink has not been reported previously.

In this work, we have mitigated the above-mentioned challenges by integrating materials science with engineering aspects. We developed an innovative approach to fabricate inkjet-printed films with on-site electrochemical sintering by diluted acetic acid to yield highly conductive and flexible Zn electrodes with low processing temperatures. The cost of the Zn raw nanomaterials is ~2 times lower compared to that of silver nanoparticles of the same morphology<sup>22</sup>. Thus, the overall costs of conductive tracks in the printed electronics applications may be decreased down up to 2 times of the current Ag NP-based tracks assuming the ink formulation process and other components (solvents, binders, and surfactants) remains nearly similar. Highly

concentrated (~40 wt%) inkjet printable metallic Zn NP ink is reported in this study. The sintering method results in electrical conductivity of ~10<sup>5</sup> S m<sup>-1</sup> for the printed Zn tracks which is comparable with previously reported values<sup>20,23</sup>. The entire process is suitable for thermosensitive substrates, cost-effective, rapid, minimizes alignment issues in the printing of successive layers, shortens production steps, and most importantly is an energy-efficient method. The construction of an all-Zn printed touch sensor circuit serves as a demonstration of the utilization of the Zn NPs in prospective printed electronics applications.

## RESULTS AND DISCUSSION

### Printing and curing of Zn NPs

Figure 1a summarizes the process to obtain conductive Zn printed features following a four-step process: (i) printing of Zn ink; (ii) drying the films to evaporate off the solvent: typically at 60 °C for ~1 min is sufficient to remove a liquid carrier from the film and the resulting film has sufficient mechanical stability and adhesion to the substrate but no electrical functionality at this point; (iii) overprinting of the curing ink on the dried Zn films and finally (iv) drying the films which give rise to shiny metallic color and electrical conductivity of the films depending upon the film thickness.

Formulating inkjet printable ink of nanomaterials is very challenging since inkjet printing requires the ink to have specific physical properties such as surface energy, viscosity, and density<sup>24–28</sup>. In addition to that NPs should have a narrow size and uniform distribution throughout the ink carrier to ensure good jetting<sup>6</sup>. These parameters strongly influence the process of drop formation after jet ejection. To be printable, inks must have a viscosity ( $\eta$ ), surface tension ( $\gamma$ ), and density ( $\rho$ ) within suitable ranges for a fixed nozzle diameter ( $a$ ). These parameters can be combined in a series of non-dimensional numbers: Reynolds number ( $Re$ ) and Weber number ( $We$ ), which are defined by Eqs. (1a) and (1b)<sup>2,29,30</sup>:

$$Re = (\rho va) / \eta \quad (1a)$$

$$We = v^2 \rho a / \gamma \quad (1b)$$

where  $v$  is the drop velocity after ejection from the nozzles and depends on the input voltage to the nozzles and the firing frequency. The inverse Ohnesorge number ( $Z^{-1} = Oh = \sqrt{W_e/R_e}$ ) is commonly used to predict if the ink will form stable drops and called the Fromm  $Z$  parameter. The droplets will be stable if  $1 < Z < 10^{31}$ . For a fixed nozzle diameter ( $a$ ) of  $21 \mu\text{m}$  (DMC 11610 cartridge), we formulated both the Zn ink and the acetic acid-based curing ink by adjusting the  $Z$  values using suitable amounts of surfactants, co-solvents, and binders. The surfactant helps to decrease the surface tension and to reduce the coffee-ring effect, the co-solvent is used to increase the viscosity and the binder is added to improve the mechanical integrity and adhesion to the substrate<sup>26</sup>.

An ink-jet formulation containing Zn nanoparticles is prepared by dispersing Zn nanoparticles (size  $\sim 40\text{--}60 \text{ nm}$ , see Supplementary Figs. 1 and 2) in a solvent mixture containing a polydimethylsiloxane surfactant and a polyvinyl butyral (PVB) binder. The full formulation can be found in "Methods" and all materials are used as supplied from suppliers. Viscosity and surface tension is optimized by changing the co-solvent and the surfactant contents, respectively as described in Supplementary Fig. 3a. The optimized surface tension of  $\approx 25 \text{ mN m}^{-1}$ , the viscosity of  $\approx 5 \text{ mPa s}$  at room temperature, and material density of  $\sim 40 \text{ wt\%}$ , give  $Z \approx 5.4$  (for  $a = 21 \mu\text{m}$ ) which provides suitable jetting behavior as illustrated in Fig. 1b.

The curing ink is based on an aqueous solution of acetic acid ( $\text{CH}_3\text{COOH}$ ) which also consists of ethylene glycol butyl ether as the co-solvent, Triton x-100 as the surfactant, and Xanthan gum as the rheology modifier. Both viscosity and surface tension of the curing ink could be varied by changing the co-solvent to water volume ratio and surfactant content, respectively (Supplementary Fig. 3b). The optimized room temperature values of surface tension ( $\approx 40 \text{ mN m}^{-1}$ ) and viscosity ( $\approx 5 \text{ mPa s}$ ) of the curing ink gives rise to  $Z \approx 3.8$  for  $a = 21 \mu\text{m}$ ; moreover, we observed a stable drop formation without any satellite tails and nozzle blocking (see Fig. 1b).

The shear-thinning behavior of the studied inks (Supplementary Fig. 4) shows the stable viscosities during the piezoelectric ejection from the cartridges. The set of dimensionless numbers ( $R_e$  and  $W_e$ ) allows us to define a green region as shown schematically in Fig. 1c which is called parameter space of inkjet printable fluids. The  $Z$  values should be inside this region for the inks to be inkjet printable. Regions toward the edges of the phase diagram are not suitable for inkjet printing either due to splashing on the substrate, or satellite drops formation, or too high ink viscosity<sup>27</sup>. Figure 1c shows that both the developed inks are well inside the green region indicating the stable printability of the inks.

The splat diameter (deposited drop size) is an important parameter that affects the continuity and integrity of the printed layer and depends on the surface energies of the substrate and the droplets, substrate temperature, and the print height (between the nozzle and the substrate)<sup>28</sup>. The drop size is investigated by jetting individual drops on the substrates and measuring their diameters using an in-built fiducial camera. Figure 1d illustrates the distribution of the Zn ink drop-sizes (splat diameter) printed on PET substrates using 20 V jetting-voltage and dried (substrate temperature:  $60^\circ\text{C}$ ). The average splat size ( $\approx 58 \mu\text{m}$  in this case) allows us to determine the drop-spacing of the Zn droplets onto the substrates and thus the overall ink consumption (inset of Fig. 1e). The drop spacing affects the uniformity, width, and thickness of the printed patterns and therefore requires careful optimization. With increased drop spacing, ink consumption is minimal. However, it gives rise to thinner films (wet thickness) and non-uniform patterns. Low drop spacing allows us to obtain uniform print patterns and thicker films, although the ink consumption is higher and sometimes worsens the resolution of the printed features. Therefore, the

choice of the drop spacing is crucial to obtain the high resolution and desired thickness of the printed films (see Supplementary Fig. 5a). In this work, we used  $30 \mu\text{m}$  drop-spacing for printing Zn ink on PET substrates, which also allows us to obtain a higher resolution of the printed patterns as observed in Supplementary Fig. 6. It is noteworthy that the droplet formation after ejection from the nozzles depends on the applied waveforms on the inks. Supplementary Fig. 5b shows the customized waveforms both for the Zn and the curing inks for stable droplet ejections.

Obtaining thicker films using a single printing pass is highly favorable for inkjet printing since it reduces fabrication time and cost. With the number of printing passes the thickness ( $t$ ) of the Zn films is changed as shown in Fig. 1e. We observe a thicker film with just a single printing pass ( $\approx 5 \mu\text{m}$ ) compared to the commonly reported thickness values by inkjet printing method<sup>26</sup>. This is primarily due to the higher material density in the Zn droplets ( $\sim 40 \text{ wt\%}$ ) and lower drop-spacing used in this study since the thickness of the printed films heavily depends on the ink concentration<sup>26</sup>. The observed single layer thickness matches fairly well with the theoretical prediction as described in Supporting information. A nearly linear increase of the film thickness with the number of printed layers is observed. It is to be noted that a slight increase ( $\sim 6\%$ ) in the Zn film thickness is observed (see Supplementary Fig. 7) after curing with acetic acid ink which is due to the swelling of the films that could be also appreciated with an optical microscope inspection.

### Optimization of curing conditions

We have optimized the acetic acid concentration in the curing ink to achieve the highest possible conductivity for the printed Zn films. Test patterns used in this evaluation are square ( $1.5 \times 1.5 \text{ cm}^2$ ) sized samples consisting of 2-printed layers of the Zn ink on PET substrates (Supplementary Fig. 5c). The samples are dried at  $60^\circ\text{C}$  on the printer stage followed by single over-layer printing of the curing ink. The sheet resistance ( $R_s$ ) has been measured using a four-point probe technique after drying the samples on the printer stage. Figure 2a summarizes the electrical properties of printed Zn patterns when cured with different acid concentrations. In the plot of the sheet resistance ( $R_s$ ) as a function of the acetic acid concentration in the curing ink four distinct zones are visible (Fig. 2a).  $R_s$  is infinite when the samples are not cured and when concentrations of acetic acid higher than  $\sim 40\%$  are used. When the printed Zn samples are cured with the curing ink firstly their  $R_s$  values reduce sharply (zone I), down to four orders of magnitude, with the increase of the acetic acid concentration in the curing ink. The nanoparticles are sintered locally by creating small bridges between the particles providing the electrical functionality to the film at the macro-scale.  $R_s$  value stabilizes when the acid concentration reaches 3 wt% and remains stable up to 10 wt% (zone II). This corresponds to the electrical conductivity of  $\sim 10^5 \text{ S m}^{-1}$ . When the acetic acid concentration is further increased, we observe an exponential rise (zone III) of the  $R_s$  values until the film becomes non-conductive again. The  $R_s$  values then stabilize after cured by 40 wt% acids (zone IV). It is noteworthy that, the  $R_s$  values are minimal when a single layer of the curing agent is over-printed on Zn samples. It increases sharply and becomes less conductive again when several acid layers are printed subsequently on the same Zn sample as illustrated in Supplementary Fig. 8 in the Supporting information. To analyze the effect of a further thermal annealing step on the electrical characteristic of Zn films cured (5 wt% acetic acids) and dried ( $60^\circ\text{C}$ );  $R_s$  measurements of films exposed in a convection oven, at increased temperatures are performed (Inset of Fig. 2a). No further reduction in the  $R_s$  values is recorded when annealing at elevated temperatures (up to  $100^\circ\text{C}$ ) is performed, on the contrary, a rise (from  $\sim 1 \Omega \text{ square}^{-1}$  to  $\sim 32 \Omega \text{ square}^{-1}$ ) of the  $R_s$  values is observed when the temperature goes beyond  $100^\circ\text{C}$  and



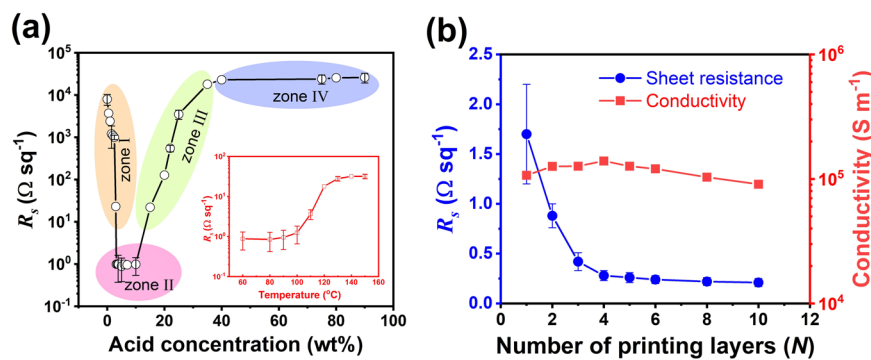


**Fig. 2 Optimization of the curing conditions.** **a** Sheet resistance variation with different acid concentrations inside the curing reagent. The samples are dried on the printer stage at 60  $^{\circ}\text{C}$  (inset: effect of post-annealing of the sample cured by 5 wt% acids. Lines are guided for the eye). **b** Variations of the sheet resistance and the electrical conductivity with a number of printed layers where samples are cured by 5 wt% acid at 60  $^{\circ}\text{C}$ . The error bars presented in the plots are standard deviations of the respective measurements. Lines are guides for the eye.

stabilizes after 130  $^{\circ}\text{C}$ . This is possibly due to the melting of the PVB polymer (m.p. 90–120  $^{\circ}\text{C}$ ) present in the Zn ink and the breaking of the bridges between the Zn NPs which makes them less conductive films. The optimization process shows that it is possible to cure the printed Zn layers by single over-layer printing of low concentration of acetic acid (~5 wt%) at low temperature (~60  $^{\circ}\text{C}$ ), which is important for uses in flexible electronics where curing temperature is a significant parameter. Figure 2b shows the variation of both the  $R_s$  values and electrical conductivity of the cured Zn samples with a number of printed layers. When the thickness of the printed films is lower, we observe a monotonic reduction of  $R_s$  values with an increasing number of printed layers (i.e., film thickness). For greater thicknesses (>4 printing layers) the sheet resistance becomes saturated and follows a power law equation<sup>32</sup>. The electrical conductivity of the films remains nearly constant ( $\sim 10^5 \text{ S m}^{-1}$ ) for the Zn samples which are 2 orders of magnitude lower than the bulk Zn conductivity ( $1.6 \times 10^7 \text{ S m}^{-1}$ )<sup>33</sup>. The electrical conductivity value is in good agreement with previously reported screen printed and aerosol jet printed Zn inks<sup>20,23</sup>.

### Morphological and structural characterizations

SEM characterizations have been carried out to visualize the effect of the acid concentration on the morphology of the cured Zn NPs. Three different samples are investigated: (i) un-cured Zn, (ii) Zn cured by 5 wt% acetic acid ink, and (iii) Zn cured by 80 wt% acetic acid ink. Figure 3a shows the SEM topographical image of uncured printed (2-printed layers) and dried (at 60  $^{\circ}\text{C}$ ) Zn ink. The sample (Fig. 3a), consisting of overlapping discrete NPs, is electrically non-conductive due to the native oxide passivation layer and which acts as an insulation between two consecutive nanoparticles. Figure 3b shows the SEM image of a similar sample following curing with 5 wt% acetic acid ink: clearly merging of the nanoparticles can be seen with the formation of nano-sized pores due to shrinkage of interparticle distance. Neck formation between two nearby particles is also visible (see Supplementary Fig. 9 in supporting document) as reported by Lee et al.<sup>20</sup> which makes the films highly conductive. We also note some amount of flaky structures on parts of the sample surfaces which is possibly due to the formation of  $(\text{Zn}(\text{ac})_2)$  during the electrochemical reaction and is appreciated by the FTIR analysis described below. Figure 3c illustrates the SEM image of a Zn film cured with 80 wt% acetic acid ink; the film is non-conductive (Fig. 2a) and characterized by the formation of nanosized crystals on top of the printed Zn layer.

We investigated by energy-dispersive X-ray spectroscopy (EDX) some of the samples taken from different zones of Fig. 2a which are cured in different ways to estimate the atomic percentage of different elements before and after the curing process. As seen

from the C/Zn and O/Zn ratios in Fig. 3d, the as printed uncured Zn NPs are initially enclosed by passivation layers which consist primarily of ZnO and  $\text{Zn}(\text{OH})_2$  and carbonyl groups (from either surfactant or the binder) which is responsible for the non-conductive nature of the non-sintered Zn films. From Fig. 3d, it is observed that when Zn film is exposed to 3–10 wt% acetic acid, both the amounts of C and O reduce drastically compared to that of un-cured Zn samples. This is because ZnO and  $\text{Zn}(\text{OH})_2$  are easily soluble in acidic solutions. The curing agent reduces the native passivation layers on the Zn NP surface through an electrochemical process. The dissolved Zn-ions are subsequently re-deposited on the nanoparticle body leaving more exposed metallic Zn surfaces to form bridges between the Zn NPs. This is the basis of the electrical functionality of the film at the macro-scale and is reported in detail previously by Lee et al. and Jayasayee et al.<sup>20,21</sup>. Simultaneously the external ZnO passivation layer could become thinner so that the metal Zn NPs underneath can be reached by the measurement probes leading to the net increase of electrical conductivity. These results are consistent with the formation of metallic Zn NP bridges (Fig. 3b) with high electrical conductivity. With the increased concentration of the acetic acid in the curing ink (>10 wt%), both C/Zn and O/Zn ratios increase again like the variation observed in zone III and zone IV in Fig. 2a. It is attributed to the precipitation of  $(\text{Zn}(\text{ac})_2)$  flakes (Fig. 3c); indicated by the significant increase in the O and C signals compared to Zn (Supplementary Table 1 in Supporting information), hindering in this way the formation of metallic Zn, which drastically reduce the electrical conductivity of the samples.

A qualitative analysis of the cured and un-cured Zn samples is carried out by FTIR measurements to confirm the mechanism described above. The observed peaks in Fig. 3e reveal that the characteristics functional group are present in the uncured and cured printed Zn NPs. The absorption peaks are found in the range of 435  $\text{cm}^{-1}$ , 520  $\text{cm}^{-1}$ , 611  $\text{cm}^{-1}$ , 620  $\text{cm}^{-1}$ , 680  $\text{cm}^{-1}$ , 800  $\text{cm}^{-1}$ , 877  $\text{cm}^{-1}$ , 948  $\text{cm}^{-1}$ , 997  $\text{cm}^{-1}$ , 1028  $\text{cm}^{-1}$ , 1114  $\text{cm}^{-1}$ , 1260  $\text{cm}^{-1}$ , 1417  $\text{cm}^{-1}$ , 1566  $\text{cm}^{-1}$ , 2360  $\text{cm}^{-1}$ , 2926  $\text{cm}^{-1}$ , 3220  $\text{cm}^{-1}$ , 3437  $\text{cm}^{-1}$ , 3480  $\text{cm}^{-1}$ . A broad absorption peak centered at 435  $\text{cm}^{-1}$ , and 520  $\text{cm}^{-1}$  is observed only in the un-cured Zn NPs which belong to the reported region of metal-oxygen in the literature and corresponds to the lattice vibrations of ZnO (Zn–O stretching vibrations)<sup>34–37</sup>. This peak belongs to the native ZnO passivation layer on the Zn NPs. The small absorption peak at 680  $\text{cm}^{-1}$  corresponds to Zn–O deformation vibrations. The observed zinc–oxygen frequency is in good agreement with the values reported in the literature<sup>38</sup>. This small peak is only observed in the acetic-acid-treated samples (5 and 80 wt%) which indicates either the existence of the native ZnO layer that is not dissolved during the acetic acid treatment or reaction of the Zn with oxygen in the environment to produce a thin ZnO layer on

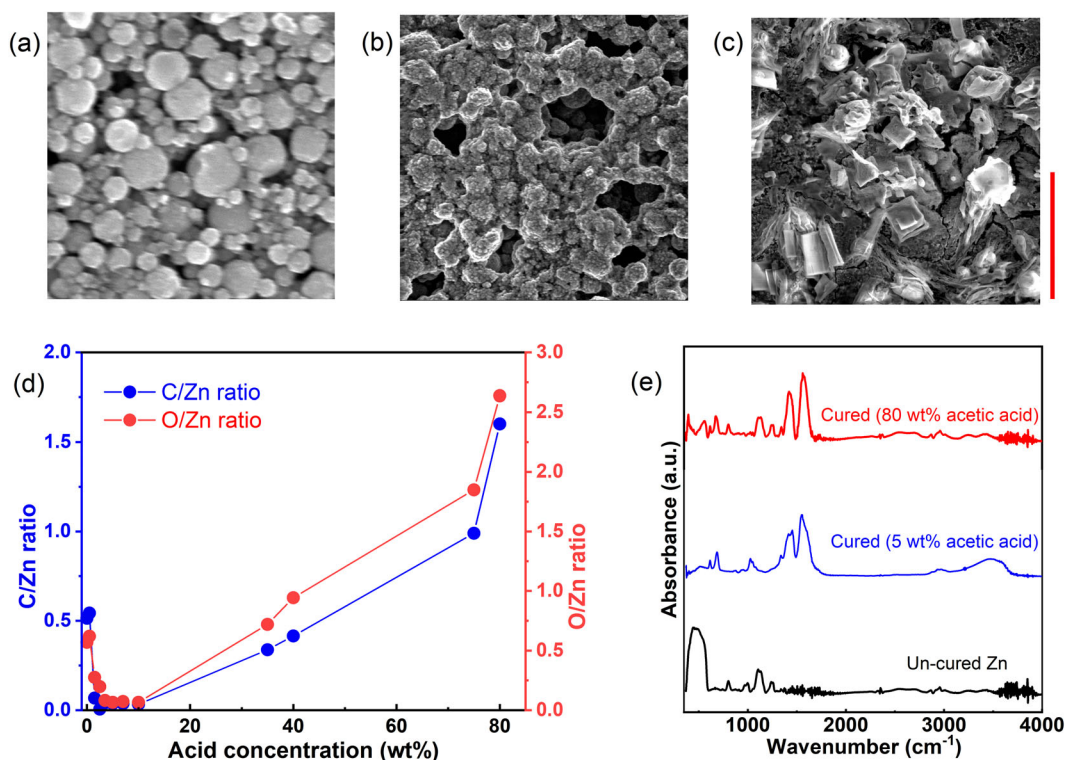


**Fig. 3** Characterization of the curing process. **a–c** SEM topography images (scale bar: 1  $\mu\text{m}$ ): **(a)** un-cured printed Zn; **(b)** Zn sample cured by 5 wt% acetic acid ink; **(c)** Zn sample cured by 80 wt% acetic acid ink. **d** EDX analysis of atomic percentage for cured and un-cured samples. Lines are guides for the eye. **e** Shows the FTIR absorbance spectrum of the printed-Zn-NPs, cured (5 wt % and 80 wt%), and uncured samples.

the surface. The small peaks in the range of 800–1200  $\text{cm}^{-1}$  correspond to the ZnO surface (Zn–O) vibrations<sup>37</sup>, and/or corresponds to the water adsorption on the zinc surface (O–H stretching and deformation)<sup>38</sup>, and/or assigned to the phonon mode vibrations of ZnO<sup>39</sup>. Two strong peaks are observed at 1413 and 1560  $\text{cm}^{-1}$ . These peaks appear only in the acetic-acid-treated samples. These peaks correspond to symmetric and asymmetric O–C–O stretching vibration<sup>40–43</sup> and can be related to the formation of Zinc acetates as observed in the SEM and EDX investigations. The absorption peak at 2360  $\text{cm}^{-1}$  is observed in all samples. This peak is from the spectrometer environment. It corresponds to gaseous  $\text{CO}_2$ . The broad peaks observed in the range of 2800–3700  $\text{cm}^{-1}$  are assigned to the stretching vibration of hydroxyl compounds. The broad peaks at 3437  $\text{cm}^{-1}$  and 3480  $\text{cm}^{-1}$  correspond to a variety of hydrated surface species including separate OH-groups<sup>40,44</sup>, hydrogen bond groups, O–H stretching, and deformation. The peaks at 3220 and 3437  $\text{cm}^{-1}$  are assigned to the water adsorption on the Zn surface and OH-groups associated with zinc vacancies<sup>38,40,44</sup>. These absorption peaks are stronger in the acetic-acid-treated sample which indicates the formation of more hydroxyl compounds and more hydrated surface species on the surface after the treatment.

### Stability and application of Zn NP ink

The environmental stability of the printed Zn patterns cured by the optimized conditions is investigated and summarized in Fig. 4a where the variation of the electrical conductivity is monitored as a function of time (days). Together with the printed Zn structure, an inkjet-printed 2-layer Ag sample is also included, as an example of reference material, in the study. All samples are kept inside the lab environment without any protection. The conductivity is nearly stable for several months ( $\approx 8$  months) except for a sharp degradation between 40 and 60 days; this coincided with the summer when the relative humidity rises

sharply (see Supplementary Fig. 10). Figure 4b shows the percentage change ( $\Delta R_s$ ) in the corresponding  $R_s$  values with a number of days, where  $\Delta R_s$  is defined by Eq. (2):

$$\Delta R_s(\%) = ((R_s - R_0)/R_0) \times 100 \quad (2)$$

where  $R_0$  is the initial sheet resistance for the samples. We observe a nearly  $\sim 200\%$  increase in the  $R_s$  values for Zn patterns due to the sharp increase of humidity in the environment associated with the summer days as mentioned above. A control experiment is performed to evaluate the effect of relative humidity (RH) on the conductivity and morphology of the cured Zn samples where the samples are kept inside a sealed jar with a saturated salt solution (NaCl). The saturated salt solution elevates the RH from 30% (lab environment) up to 75% at room temperature<sup>45</sup>. We observe a sharp increase ( $\sim 175\%$ ) of sheet resistance with elevated RH (see Supplementary Fig. 11). Although no visible change in the morphology is observed, there is an increase of the net oxygen content on the film surface at higher RH (Supplementary Fig. 12 and Supplementary Table 2 in the supporting document). This measurement suggests that the  $\text{ZnO}_x$  passivation layer is formed when the relative humidity is sufficiently high which affects the overall conductivity of the samples and electrodes should be protected by encapsulation layers for use in practical printed electronics applications.

The Zn ink stability is assessed by printing square patterns with the same ink cartridge for consecutive days and measuring variation in their electrical conductance (the following curing at optimal conditions), as seen from Fig. 4c. The conductance of the Zn patterns printed with the same cartridge remains constant for up to 20 consecutive days followed by rapid degradation. In this region, we observe frequent clogging of the nozzles, and several cleaning steps are required to keep the nozzles running. This behavior is possibly either due to the starting of sedimentation or agglomeration of the NPs. After 40 days, the cartridge is non-jettable anymore. This investigation indicates that there is further

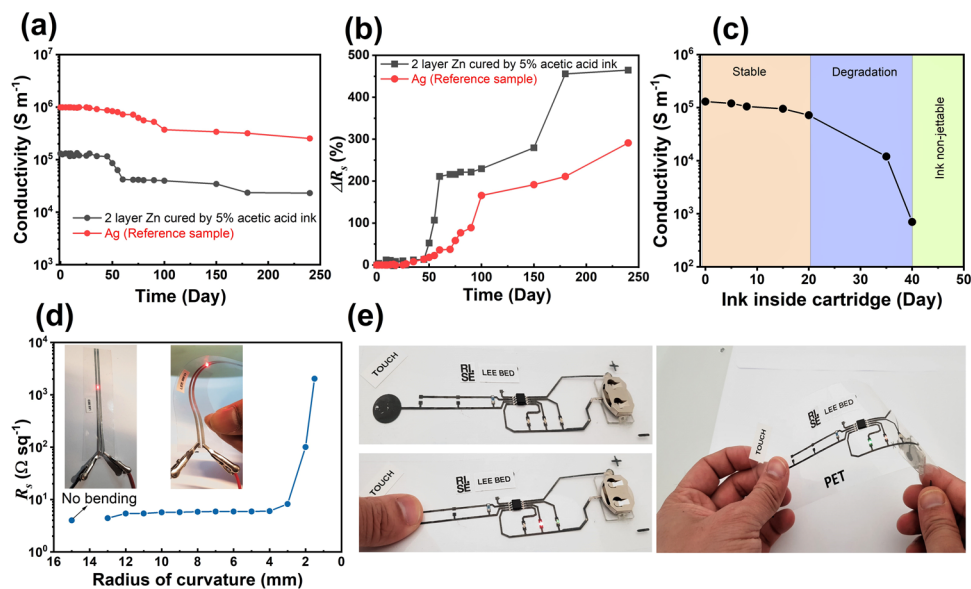


**Fig. 4 Stability and demonstration.** **a** Electrical conductance variations of chemically cured Zn patterns with time, where a printed Ag sample is shown as a reference. The Ag sample is cured at 120 °C for 30 min. **b** Percentage change of  $R_s$  for chemically cured Zn patterns with time. A printed Ag sample is shown as a reference. **c** Change of electrical conductance for Zn patterns printed with the same cartridge for several consecutive days. Lines are guides for the eye. **d** Variation of the sheet resistance of cured samples bent with different radii of curvature (Inset: mechanical flexibility of the cured Zn electrodes printed on PET substrates. The LED is mounted on top of the 2 parallel Zn tracks). **e** A demonstrator circuit on PET substrate with a touch sensor, mounted LEDs, a microcontroller, and battery.

scope to enhance the stability of the Zn ink by screening other surfactants or binders. It is to be noted that the acetic acid-based curing ink is sufficiently stable up to several months and no degradation in the jetting behavior is observed. It is worth mentioning that the ink-jetting behavior remains stable when the cartridge head is heated up to 40 °C indicating the heat stability of the Zn NP ink formulation.

The mechanical flexibility of the cured Zn patterns is investigated and shown in Fig. 4d where the variation of the  $R_s$  values is illustrated with different bending curvatures of the samples. Square-sized (2.0 × 2.0 cm<sup>2</sup>) Zn samples are printed and cured (at optimal conditions) on PET substrates and bent by a custom-made tool having various radii of curvature. We observe a sharp (~35%) increment of the  $R_s$  values when bent with a 12 mm radius of curvature as compared to the initial  $R_s$  of the samples and thereafter, it shows stable  $R_s$  values with decreased radii of curvature until 3 mm. We also noticed a sharp rise of  $R_s$  values when bent with <3 mm, radii of curvature because of the crack formation on the films as seen visibly by optical microscope and from the SEM cross-sectional image (see Supplementary Fig. 13). This observation implies that the cured Zn electrodes/patterns are mechanically flexible until a critical point of curvature and there is a possibility for further improvement of the robustness of the ink adjusting the formulation components. The mechanical pliability of the cured Zn electrodes is further illustrated in the inset of Fig. 4d where a LED is mounted between two parallel Zn tracks/ electrodes printed and cured by inkjet printing method (line width 0.5 mm and gap between lines 0.2 mm). With proper input voltage, the LED can be illuminated, and its brightness remains unchanged when the printed circuit is folded or bent in any direction, hinting at the mechanical robustness of the cured Zn films.

Figure 4e demonstrates inkjet-printed and chemically cured Zn-based conductive tracks forming a touch sensor circuit. The commercial low power microcontroller is used that operates without external active electronic components and programmed as per the principle described elsewhere<sup>46</sup>. The touchpad (circular area) serves as a point-of-body coupled capacitive component. A resistor between the touchpad and the second pin of the

microcontroller forms an RC circuit. Upon touching the touchpad the three LEDs are turned ON sequentially (see Supporting video). A 3 V CR3032 battery powered the circuit demonstrating a low power functional printed circuit. The current consumption, while all LEDs are ON, is measured to be around ~1.3 mA while the circuit consumed ~0.8 mA when LEDs were OFF. The touchpad and the LEDs are functional even after bending the circuit in different axes showing the mechanical flexibility of the printed and cured Zn electrodes.

In conclusion, we have developed highly conductive inkjet printable concentrated ink based on Zn NPs as an alternative to the conventional metallic inks available for printed electronics applications. This paper describes an in situ method of chemical curing of inkjet-printed Zn NP ink at low temperature (~60 °C) without using the conventional curing methods like thermal annealing, atomic diffusion, or photonic sintering. The curing process which is based on the electrochemical reaction between the acetic acid and the native oxide layers; is in situ, energy-efficient, applicable to large-area printing, rapid, and suitable for flexible electronics applications. Systematic studies reveal the importance of acid concentration on the electrical behavior of the cured Zn NPs and highly conductive (~10<sup>5</sup> S m<sup>-1</sup>) and mechanically robust Zn patterns are achieved. Since the Zn NP ink is not suitable for an extended period of usage due to the instability of the NPs, effort should be focused on scanning other formulation components. Once a suitable formulation recipe is found for stable ink, curing conditions need to be optimized again. Finally, due to the simplicity of the process, it is envisaged that this technology has wide potential in flexible printed electronics applications.

## METHODS

### Formulation of Zn and curing inks

A premix is prepared by mixing ethylene glycol butyl ether (40.5 wt%), dipropylene glycol (17.4 wt%), and a polydimethylsiloxane surfactant BYK 333 (0.3 wt%). To this mixture 1.0 wt% PVB binder (Mowital B20H) is added under stirring. The premix is left under continuous stirring until the PVB is fully dissolved. In total, 40.8 wt% of Zn nanoparticles (purity 99.7%,



SkySpring Nanomaterial) are then added to the premix. To break up agglomerates, the Zn mixture (~25 mL volume) is sonicated with an ultrasonic probe sonicator (Fisher scientific, sonic Dismembrator, 12.7 mm probe diameter) with 200 W effective sonication power for an effective sonication time of 70 min. As temperature tends to rise during sonication the mixture is cooled externally with ice.

The curing ink is formulated by adding a suitable concentration of acetic acid to the ink solvent. The solution is bath sonicated for 30 min before printing. The ink solvent consists of 1:100 ethylene glycol butyl ether: H<sub>2</sub>O by volume, 0.005 wt% Triton x-100 (surfactant), and 0.001 wt% Xanthan gum (rheology modifier). Acetic acid (99.8% pure), surfactant, and the rheology modifier are purchased from Sigma Aldrich and all materials are used as supplied from suppliers.

### Printing and curing process

The Zn ink is printed by Dimatix DMP-2800 inkjet printer (Fujifilm Dimatix, Inc., Santa Clara, USA) on PET (Polifoil 125 μm thick) substrates using DMC 11610 cartridges which have a typical drop volume of 10 pL and 21 μm diameter spaced 254 μm apart. 30 μm drop spacing is used to print Zn patterns using ≈20 V jetting voltage and 28 °C cartridge head temperature. The jetting frequency was varied between 1 and 10 kHz. For samples described in this study, a print height (distance between the substrate and the nozzle) of 0.4–0.5 mm is used. The substrates are kept at 60 °C on the printer stage unless otherwise specified and no pre-treatment of the substrates is carried out before printing. The substrates are cleaned by ethanol washing and drying by nitrogen airgun. The printed samples are dried on the printer stage before curing by the acetic acid ink. For printing curing ink, the same type of cartridges is used with ≈16 V jetting voltage and 28 °C cartridge head temperature with 0.5 mm print height. The drop velocities for the Zn ink and the curing ink are measured to be 5 m s<sup>-1</sup> and 6.5 m s<sup>-1</sup>, respectively. The cured samples are dried on the same stage either before further annealing inside a convection oven or direct characterizations.

### Preparation of the Ag reference sample

The reference samples used in Fig. 4a, b are printed on PET substrate using commercial Ag NP inkjet ink by 10 pL cartridge through optimized printing parameters. The printed samples are cured at 120 °C for 1 h in a convection oven.

### Conductivity measurements

The sheet resistance of the printed and cured samples is measured by the in-house Ossila four-point probe system. For each average data point, four different samples (size: 1.5 × 1.5 cm<sup>2</sup>) are measured. The thickness values of the printed and cured films are investigated by an optical profilometer (Sensofar PLux neox) and reconfirmed by SEM cross-section measurements. Electrical DC conductivity is calculated by Eq. (3):

$$\text{Conductivity} = 1/(\text{Sheet resistance} \times \text{thickness}) \quad (3)$$

### Other characterizations

SEM topography and cross-section images are obtained using a field-emission scanning electron microscope (JSM-6700F, JEOL, Japan). For the higher resolution of the images 5 nm Au is deposited on some of the samples. Viscosity and surface tension of the inks have been measured using Anton Paar Modular Compact Rheometer (MCR102 rheometer with cone plate, geometry: 50 mm; 1°) and KRÜSS mobile surface analyzer, respectively. FTIR measurements are carried out using a MID-IR FTIR spectrometer (Bruker Equinox 55).

### Fabrication of the demonstrator circuit

The whole circuit is fabricated by inkjet printing 2-layer Zn ink on PET substrate which is followed by single over-layer printing of the curing ink (5 wt% acetic acid) while the substrate temperature remains at 60 °C. The printed tracks are 1 mm wide and the gap between the tracks near the microcontroller is 300 μm. The commercial low-power microcontroller and the LEDs are mounted on the conductive tracks with silver soldering paste. A 3 V CR3032 battery is connected to power the demonstrator circuit.

### DATA AVAILABILITY

The authors declare that the main data supporting the findings of this study are available within the article and its Supplementary Information file. Extra data are available from the corresponding author upon request.

Received: 30 April 2021; Accepted: 16 June 2021;

Published online: 07 July 2021

### REFERENCES

- Wu, Lei, Dong, Zhichao, Li, Fengyu, Zhou, Haihua & Song, Yanlin Emerging progress of inkjet technology in printing optical materials. *Adv. Opt. Mater.* **4**, 1915–1932 (2016).
- Abdolmaleki, Hamed, Kidmose, Preben & Agarwala, Shweta Droplet-based techniques for printing of functional inks for flexible physical sensors. *Adv. Mater.* **33**, 2006792 (2021).
- Sirringhaus, H. et al. High-resolution inkjet printing of all-polymer transistor circuits. *Science* **290**, 2123–2126 (2000).
- Dang, MauChien, Dang, ThiMy, Dung & Fribourg-Blanc, Eric Inkjet printing technology and conductive inks synthesis for microfabrication techniques. *Adv. Nat. Sci.* **4**, 015009 (2013).
- Sridhar, Ashok, Blaudeck, Thomas & Baumann, ReinhardR. Inkjet printing as a key enabling technology for printed electronics. *Mater. matters* **6**, 12–15 (2011).
- Gerard Cummins, MarcP. Y. Desmulliez, inkjet printing of conductive materials: a review. *Circuit World* **38**, 193–213 (2012).
- Tan, HongWei, An, Jia, Chua, CheeKai & Tran, Tuan Metallic nanoparticle inks for 3D printing of electronics. *Adv. Electron. Mater.* **5**, 1800831 (2019).
- Hsien-Hsueh, L., Kan-Sen, C. & Kuo-Cheng, H. Inkjet printing of nanosized silver colloids. *Nanotechnology* **16**, 2436 (2005).
- Gaspar, C., Passoja, S., Olkkonen, J. & Smolander, M. IR-sintering efficiency on inkjet-printed conductive structures on paper substrates. *Microelectron. Eng.* **149**, 135 (2016).
- Park, B. K., Kim, D., Jeong, S., Moon, J. & Kim, J. S. Direct writing of copper conductive patterns by ink-jet printing. *Thin Solid Films* **515**, 7706–7711 (2007).
- UT Dots Inc., Our Products, <https://utdots.com/products> Accessed Mar 2021.
- <https://nanomagic.com/ani/> Accessed Mar 2021.
- Segal-Scharia, M. Nano dimension announces new collaboration with Tel Aviv university enabling 3D printing of sensors using nickel nano-particles, <http://www.nano-di.com/investor-news/nano-dimension-announces-new-collaboration-with-tel-aviv-university-enabling-3d-printing-of-sensors-using-nickel-nano-particles> Accessed Mar 2021.
- Kang, J. S., Ryu, J., Kim, H. S. & Hahn, H. T. Sintering of inkjet-printed silver nanoparticles at room temperature using intense pulsed light. *J. Electron. Mater.* **40**, 2268 (2011).
- Mazumder, M., et al., Industrial production and field evaluation of transparent electrodynamic screen (EDS) film for water-free cleaning of solar collectors. in *Proc. 2019 IEEE 46th Photovoltaic Specialists Conference (PVSC)*, Chicago, IL, USA, pp. 3269–3276, <https://doi.org/10.1109/PVSC40753.2019.8980599>, 2019.
- Magdassi, S., Grouchko, M. & Kamyshny, A. Copper nanoparticles for printed electronics: routes towards achieving oxidation stability. *Materials* **3**, 4626 (2010).
- Kim, Y. J., Ryu, C.-H., Park, S.-H. & Kim, H.-S. The effect of poly (N-vinylpyrrolidone) molecular weight on flash light sintering of copper nanopaste. *Thin Solid Films* **570**, 114 (2014).
- <https://www.pvnanocell.com/gold-ink> Accessed Mar 2021.
- Li, Zheng & Suslick, KennethS. Chemically induced sintering of nanoparticles. *Angew. Chem. Int. Ed.* **58**, 14193–14196 (2019).
- Lee, YoonKyeung et al. Room temperature electrochemical sintering of Zn microparticles and its use in printable conducting inks for bioresorbable electronics. *Adv. Mater.* **29**, 1702665 (2017).
- Jayasayee, Kaushik et al. Cold sintering as a cost-effective process to manufacture porous zinc electrodes for rechargeable zinc-air batteries. *Processes* **8**, 592 (2020).
- <https://ssnano.com/> Accessed Mar 2021.
- Mahajan, B. K. et al. Aerosol printing and photonic sintering of bioresorbable zinc nanoparticle ink for transient electronics manufacturing. *Sci. China Inf. Sci.* **61**, 060412:1–060412:10 (2018).
- Baeg, K. J., Caironi, M. & Noh, Y. Y. Toward printed integrated circuits based on unipolar or ambipolar polymer semiconductors. *Adv. Mater.* **25**, 4210–4244 (2013).
- Hutchings I. M. & Martin G. D. *Inkjet Technology for Digital Fabrication* (Wiley, 2012).
- Daryl, Mc. Manus et al. Water-based and biocompatible 2D crystal inks for all-inkjet-printed heterostructures. *Nat. Nanotechnol.* **12**, 343–350 (2017).

27. Shanker, Ravi et al. Noniridescent biomimetic photonic microdomes by inkjet printing. *Nano Lett.* **20**, 7243–7250 (2020).
28. Jorge, Alamán et al. Inkjet printing of functional materials for optical and photonic applications. *Materials* **9**, 910 (2016).
29. Derby, B. Inkjet printing of functional and structural materials: fluid property requirements, feature stability, and resolution. *Annu. Rev. Mater. Res.* **40**, 395–414 (2010).
30. Jang, D., Kim, D. & Moon, J. Influence of fluid physical properties on ink-jet printability. *Langmuir* **25**, 2629–2635 (2009).
31. Reis N. & Derby B., Ink jet deposition of ceramic suspensions: modeling and experiments of droplet formation, *MRS Online Proc. Lib. Arch.*, 625,117, 2000.
32. D. R. Gamota, P. Brazis, K. Kalyanasundaram, & J. Zhang, *Printed Organic and Molecular Electronics*, (Kluwer Academic Publishers, 2004), ISBN: 1 4020 7707 6. <https://www.thoughtco.com/table-of-electrical-resistivity-conductivity-608499>.
34. Ansari, S. G. et al. Effect of nanostructure on the urea sensing properties of sol–gel synthesized ZnO. *Sens. Actuator B-Chem.* **137**, 566 (2009).
35. Vajargaha, P. H., Abdizadeha, H., Ebrahimifarda, R. & Golobostanfarda, M. R. Sol–gel derived ZnO thin films: Effect of amino-additives. *Appl. Surf. Sci.* **285**, 732 (2013).
36. Yu, Hou-Yong, Chen, Guo-Yin, Wang, Yi-Bo & Yao, Ju-Ming A facile one-pot route for preparing cellulose nanocrystal/zinc oxide nanohybrids with high antibacterial and photocatalytic activity. *Cellulose* **22**, 261–273 (2015).
37. Davydov A., *Molecular Spectroscopy of Oxide Catalyst Surfaces* (Wiley, 2003), ISBN: 9780471987314.
38. Kumar, Harish & Rani, Renu Structural and optical characterization of ZnO nanoparticles synthesized by microemulsion route. *Int. Lett. Chem. Phys. Astron.* **14**, 26–36 (2013).
39. Boccuzzi, F., Morterra, C., Scala, R. & Zecchina, A. Infrared spectrum of microcrystalline Zinc Oxide. electronic and vibrational contributions under different temperature and environmental conditions. *J. Chem. Soc. Faraday Trans. 2*, 2059–2066 (1981).
40. Keyes, B. M., Gedvilas, L. M., Li, X. & Coutts, T. J. Infrared spectroscopy of polycrystalline ZnO and ZnO:N thin films. *J. Cryst. Growth* **281**, 297–302 (2005).
41. Boccuzzi, F., Borello, E., Chiorino, A. & Zecchina, A. IR detection of surface microscopic modes of microcrystalline ZnO. *Chem. Phys. Lett.* **61**, 617–619 (1979).
42. Saussey, J., Lavalley, J. C. & Bovet, C. Infrared study of CO<sub>2</sub> adsorption on ZnO. Adsorption sites. *J. Chem. Soc. Faraday Trans. 1*, 1457–1463 (1982).
43. Shamhari, NuraqeelahMohammad, Wee, BoonSiong, Chin, SukFun & Kok, KuanYing Synthesis and characterization of zinc oxide nanoparticles with small particle size distribution. *Acta Chim. Slov.* **65**, 578–585 (2018).
44. Atherton, K., Newbold, G. & Hockey, J. A. Infra-red spectroscopic studies of zinc oxide surfaces. *Discuss. Faraday Soc.* **52**, 33–43 (1971).
45. <https://studylib.net/doc/18269014/saturated-salt-solutions>.
46. <https://playground.arduino.cc/Main/CapacitiveSensor>.

## ACKNOWLEDGEMENTS

The authors would like to thank the LEE-BED project funded by European Union's Horizon 2020 research and innovation program under grant agreement number 814485.

The authors also thank Xin Wang and Olle Hagel (both from RISE Research Institutes of Sweden) for optical profilometer measurements of film thickness and for mounting the LED on printed Zn electrodes, respectively. The authors acknowledge useful discussions with Anwar Ahniyaz and Petru Niga from RISE Research Institutes of Sweden.

## AUTHOR CONTRIBUTIONS

P.J.W. and P.D. conceived the original idea of the project. S.M. formulated the curing ink, carried out the inkjet printing, electrical and optical characterizations, interpreted the data, and wrote the manuscript through contributions of all authors. M.K. carried out the Zn ink formulation and rheology measurements at the initial stage of the project which was followed by A.S. at the later stage. N.H.A. performed the SEM, EDX, and FTIR measurements. Y.M. assisted in designing the test structures and designed and fabricated the demonstrator circuits. V.B. contributed to the interpretation of different data and discussions. All works were coordinated by D.N. All authors have approved the final version of the manuscript.

## COMPETING INTERESTS

The authors declare no competing interests.

## ADDITIONAL INFORMATION

**Supplementary information** The online version contains supplementary material available at <https://doi.org/10.1038/s41528-021-00111-1>.

**Correspondence** and requests for materials should be addressed to Subimal Majee or David Nilsson

**Reprints and permission information** is available at <http://www.nature.com/reprints>

**Publisher's note** Springer Nature remains neutral with regard to jurisdictional claims in published maps and institutional affiliations.



**Open Access** This article is licensed under a Creative Commons Attribution 4.0 International License, which permits use, sharing, adaptation, distribution and reproduction in any medium or format, as long as you give appropriate credit to the original author(s) and the source, provide a link to the Creative Commons license, and indicate if changes were made. The images or other third party material in this article are included in the article's Creative Commons license, unless indicated otherwise in a credit line to the material. If material is not included in the article's Creative Commons license and your intended use is not permitted by statutory regulation or exceeds the permitted use, you will need to obtain permission directly from the copyright holder. To view a copy of this license, visit <http://creativecommons.org/licenses/by/4.0/>.

© The Author(s) 2021, corrected publication 2021